J. Fluid Mech. (1998), *vol.* 361, *pp.* 309–331. Printed in the United Kingdom

Dispersion of a ball settling through a quiescent neutrally buoyant suspension

By JAMES R. ABBOTT[1], ALAN L. GRAHAM[1], LISA A. MONDY[2] AND HOWARD BRENNER[3]

[1] Los Alamos National Laboratory, Los Alamos, NM 87545, USA

[2] Sandia National Laboratories, Albuquerque, NM 87185-0834, USA

[3] Massachusetts Institute of Technology, Cambridge, MA 02139-4307, USA

(Received 11 July 1997 and in revised form 16 December 1997)

Individual falling balls were allowed to settle through otherwise quiescent well-mixed suspensions of non-colloidal neutrally buoyant spheres dispersed in a Newtonian liquid. Balls were tracked in three dimensions to determine the variances in their positions about a mean uniform vertical settling path. The primary experimental parameters investigated were the size of the falling ball and the volume fraction and size of the suspended particles. Unlike the horizontal variances, the vertical variances were found to be affected by short-time deterministic behaviour relating to the instantaneous local configurational arrangement of the suspended particles. For sufficiently long intervals between successive observations, the trajectories of the balls were observed to disperse about their mean settling paths in a random manner. This points to the existence of a Gaussian hydrodynamic dispersivity that characterizes the linear temporal growth of the variance in the position of a falling ball. The functional dependence of these horizontal and vertical dispersivities upon the parameters investigated was established.

The dispersivity dyadic was observed to be transversely isotropic with respect to the direction of gravity, with the vertical component at least 25 times larger than the horizontal component. The vertical dispersivity $\hat{D}_v$ (made dimensionless with the diameter of the suspended spheres and the mean settling velocity) was observed to decrease with increasing falling ball diameter, but to decrease less rapidly with concentration than theoretically predicted for very dilute suspensions; moreover, for falling balls equal in size to the suspended spheres, $\hat{D}_v$ increased linearly with increasing volume fraction ϕ of suspended solids.

In addition to the above experiments performed on suspensions of spheres, previously published settling-velocity data on the fall of balls through neutrally buoyant suspensions of rods possessing an aspect ratio of 20 were re-analysed, and vertical dispersivities calculated therefrom. (These data, taken by several of the present investigators in conjunction with other researchers, had only been grossly analysed in prior publications to extract the mean settling velocity of the ball, no attempt having been made at the time to extract dispersivity data too.) The resulting vertical dispersivities, when rendered dimensionless with the rod length and mean settling velocity, showed no statistically significant dependence upon the falling-ball diameter; moreover, all other things being equal, these dispersivities were observed to increase with increasing rod concentration.

1. Introduction

Hydrodynamic forces govern particle–particle interactions in concentrated suspensions at low Reynolds numbers. While the macroscale behaviour of the suspension may be that of a hypothetical homogeneous Newtonian liquid, individual particles at the microscale pursue chaotic trajectories about the mean (macroscale) particle motion predicted on the basis of this hypothetical Newtonian fluid. In simple shear flows with uniform shear rates, this leads to behaviour characterized by a self-diffusion coefficient for the suspended spheres with no tendency towards non-uniform spatial particle distributions (Eckstein, Bailey & Shapiro 1977; Leighton & Acrivos 1987*a*; Nadim 1988). In contrast, for inhomogeneous shear fields such as Poiseuille flows, the particles tend to migrate to the low-shear-rate regions of the flow (Gadala-Maria & Acrivos 1980; Leighton & Acrivos 1987*b*; Graham *et al.* 1991; Abbott *et al.* 1991; Phillips *et al.* 1992; Wang, Mauri & Acrivos 1993). Additionally, Ham & Homsy (1988), Nicolai *et al.* (1995), Nicolai, Peysson & Guazzelli (1996) studied the motion of a tracer particle in non-neutrally buoyant suspensions undergoing sedimentation. A recent IUTAM symposium on the subject of hydrodynamic diffusion in suspensions is summarized by Davis (1996).

This paper describes experiments that involve tracking the trajectory of a single settling ball through an otherwise quiescent suspension of neutrally buoyant spheres (in addition to the re-analysis of comparable data on rod suspensions). The discrete nature of the suspensions was readily apparent from the ball's motion when the ball was of a size comparable to that of the suspended particles. Instead of ultimately reaching (and subsequently maintaining) a constant terminal velocity, as in a true fluid continuum, the falling ball settles erratically through the suspended particles, albeit at a well-defined mean settling velocity, despite large fluctuations in its *instantaneous* velocity. The chaotic portion of the observed behaviour results from hydrodynamic interactions between the settling ball and the suspended particles, as well as from the interactions among the suspended particles themselves. Periods of almost no motion, occurring as the ball collides with and eventually moves around suspended particles, alternate with periods of relatively high velocity, occurring as the ball settles through the interstitial fluid between particles.

Davis & Hill (1992) proposed a theoretical model for the hydrodynamic dispersion of a falling ball settling through a neutrally buoyant suspension of spherical particles. Their model considers only two-body interactions between the settling sphere and a suspended sphere, and, hence, is limited to dilute suspensions. Furthermore, it assumes *a priori* that a random arrangement of suspended spheres will lead to a Fickian process, wherein the average second central moment (variance) of the instantaneous position of the settling ball increases linearly with time. Analogous to the molecular diffusivity of Brownian particles in homogeneous fluids, a dispersion coefficient is defined which is equal to one-half the slope of this variance with respect to time. In addition to the prediction of a linear dependence upon solids volume fraction ϕ, the dispersivity is further predicted by Davis & Hill (1992) to scale approximately inversely with the size of the settling ball relative to the suspended spheres. Because of the reversible nature of two-body interactions, their model predicts no net horizontal excursions, and hence no horizontal dispersivity. Here, we focus experimentally on the three-dimensional dispersion of a falling ball settling through a suspension of neutrally buoyant spheres or rods.

Nicolai *et al.* (1996) performed experiments involving sedimenting suspensions, wherein the spherical tracer particle ('falling ball') varied in both size and density

relative to the sedimenting spheres. While they examined the fluctuating behaviour of these tracer particles, their study focuses on balls that settled faster than the sedimenting suspension. However, the time scales of the settling ball and the suspension were still comparable.

A principal objective of our experiments was to test whether the observed fluctuations in the ball's settling velocity could be interpreted as a Fickian process and, if so, to extract from the trajectory data the functional dependence of the resulting falling-ball dispersivities upon the various parameters characterizing the process. The primary experimental parameters investigated were the sizes of the settling ball and suspended particles, as well as the concentration and geometry (spheres vs. rods) of the latter. Since the present data for the spheres were taken under more optimal conditions than prevailed for the older rod data (Milliken *et al.* 1989*a*, *b*) – see § 4 of the present paper, and since the later sphere data were taken using two horizontal camera angles (so as to allow the measurement of horizontal dispervities in addition to the vertical dispersivities) rather than a single camera angle, our focus and emphasis in the subsequent description will be on the sphere data. The rod data, while more limited in scope (i.e. possessing sensors whose configration was such that only vertical ball positions, and hence, ultimately, vertical dispersivities, could be measured) and accuracy, will nevertheless be briefly commented upon in § 4.

For sufficiently long times the variances were observed to grow linearly with time, as is characteristic of a Fickian process. Because the settling balls in these experiments were comparable in size to the suspended spheres, it was possible to observe during the course of a single experiment a temporal transition. Initially, the ball settled deterministically past a particular local arrangement of spheres, ultimately transitioning to a random process arising from the ball settling past an ensemble of many such local arrangements. Deterministic effects were observed to result in quadratic growth of the variances, in contrast to stochastic effects, which resulted in linear growth.

Section 2 describes the experimental design for the sphere data. This includes a description of the equipment and suspensions employed, as well as the experimental protocol for determining the instantaneous position of the settling ball from two non-collinear camera views. In optically transparent suspensions, wherein the refractive index of the suspending fluid is matched with that of the suspended particles, the falling balls were observed visually. For opaque suspensions, observations were made using real-time radiography. In both cases the density of the suspending liquid matched that of the suspended particles, so that no significant settling (or rising) of the suspended particles occurred over the time scale of the experiments. A nonlinear conversion algorithm was used to accurately determine the instantaneous three-dimensional location of the centre of the settling ball from two orthogonal camera views of its position.

Section 3 describes the experimental data reduction and interpretation for suspensions of spheres. These new measurements of detailed settling paths were used to determine variances in the three coordinates which define the centre of the falling ball as a function of time. These trajectories served to determine the variances and, concomitantly, to test the hypothesis that the dispersion phenomenon is, in fact, an uncorrelated random process.

In an attempt to separate the long-term random processes from the shorter-term deterministic effects, several numerical 'experiments' were performed and interpreted. In these experiments a Fickian process was assumed to govern the motion of the settling ball. In this manner an appropriate methodology was established for properly sampling the experimentally measured trajectories.

Because a purely Fickian process displays only linear growth of the variances with time, any nonlinear behaviour – manifested by nonlinear growth of the variances – would necessarily reflect the presence of additional physical processes. To account for the nonlinear behaviour of the variances observed in our experiments, a model incorporating a relaxation time is proposed to account for the experimentally observed temporal behaviour of the falling-ball trajectories. Using physical arguments, the time scale over which the short-term nonlinear behaviour is expected to be important is estimated, and subsequently used to extract the long-term dispersivity from the raw data. Also discussed are the methods employed for establishing error limits on the variances and dispersivities.

Explicit results are presented in § 3 for the (non-dimensional) vertical and horizontal dispersivities, $\hat{D}_v$ and $\hat{D}_h$, respectively (made dimensionless with the falling ball's average settling velocity $\overline{U}$ and the diameter d_s of the suspended spheres). In particular, variances together with the resulting dispersivities are depicted graphically as functions of falling-ball diameter d_f and density ρ_f, as well as of the volume concentration ϕ of suspended spheres. At moderate concentrations our measurements revealed the existence of a small but measurable $\hat{D}_h$, which was at least 25 times smaller than $\hat{D}_v$. The vertical dispersivity $\hat{D}_v$ displays a variable dependence upon the ratio d_f/d_s of falling-ball to suspended-sphere diameter. At low solids concentrations, $\hat{D}_v$ depends almost inversely on the ratio d_f/d_s. This dependence decreases with increasing ϕ, until at $\phi = 0.50$ the vertical dispersivity becomes almost independent of d_f/d_s. For circumstances where $d_f/d_s \approx 1$, $\hat{D}_v$ increased approximately linearly with ϕ.

Section 4, which deals with the older rod data, describes a method for estimating the vertical dispersivity from the observed variations in settling velocity reported by Milliken *et al.* (1989*a*, *b*) for suspensions of rods. Dispersivities obtained thereby were observed to increase with increasing rod concentration, with no significant dependence upon the falling-ball diameter. However, the latter was always less than the length of the suspended rods.

Finally, § 5 provides a summary and discussion of our main conclusions.

2. Experimental method for sphere suspensions

2.1. *Suspensions and apparatus*

The suspensions employed in the experiments consisted of polymethyl methacrylate (PMMA) spheres suspended in viscous Newtonian fluids. These particles were neutrally buoyant in the suspending liquid described below, and were sufficiently large to assure that colloidal and Brownian forces could not appreciably affect suspension behaviour. Two separate suppliers furnished the PMMA spheres. The first set consisted of Diakon MG102 particles (ICI-United Kingdom, London) with a mean diameter of 675 μm. These were sieved, and the mean diameter of the sieved particles taken to be the arithmetic average (655 μm) of the mesh sieve sizes on which the particles were collected (600 μm) and that lying above it (710 μm). The resultant size distribution of the sieved samples corresponded to a standard deviation of approximately 5% of the average sphere diameter. A suspension of these spherical particles in a fluid whose material properties are described below was prepared at a solids volume concentration of $\phi = 0.15$.

The second set of spheres consisted of individually ground 3.175 mm diameter spheres (Engineering Laboratories Inc., Pompton Lakes, NJ). Published tolerances on

these larger spheres ($\pm$0.05 mm variation in diameter and $\pm$0.025 mm in sphericity) correspond to a standard deviation of less than 1% in the average sphere diameter. Suspensions of these particles in the fluid described below were prepared at concentrations of $\phi = 0.15$, 0.30, and 0.50.

The fluid used in our experiments, which matched both the density and refractive index of the suspended PMMA spheres, consisted of a mixture of 1,1,2,2 tetrabromoethane (TBE, Eastman Kodak, Rochester, NY), polyethylene glycol (90 000 UCON oil, Union Carbide Corp., Danbury, CT), and alkylaryl polyether alcohol (Triton X-100, J. T.. Baker, Phillipsburg, NJ). Relative proportions of each of these three liquids were 14.07, 35.66, and 50.27% by weight, respectively. The fluid also contained about 0.1% by weight of Tinuvin 328^{TM} (Ciba-Geigy Co., Ashley, NY) which was added to the TBE as an antioxidant to prevent rapid discoloration of the fluid (due either to ultraviolet light or contact with metals, especially iron alloys).

The fluid composition was such that the resulting density nominally matched that of the PMMA particles, namely about 1.182 g cm^{-3}. Once a solution was prepared, the temperature at which the fluid density most closely matched that of the particles was determined by finding the temperature at which a small sample of the PMMA particles remained suspended. Use of an mgw Lauda RCS 20-D water bath (Brinkmann Instruments Co., Houston, TX) enabled the temperature to be controlled to within $\pm$0.03 °C, making it possible to maintain a set of particles in suspension for several days. However, PMMA particles of different sizes or shapes, or from different batches, were observed to possess slightly different buoyancies than the average. Nevertheless, during a 24-hour period the suspended particles did not noticeably settle or rise.

The temperature at which our fluid density most closely matched that of the particles was 22.95 °C, at which temperature the fluid viscosity was 4.52 Pa s^{-1}.† The Newtonian behaviour and resulting viscosity were verified using a Carri-Med Controlled Stress Rheometer (TA Instruments, New Castle, DE). The refractive index of this fluid (namely, 1.491) also matched that of the PMMA particles.

Suspensions were prepared by initially introducing the particles into the suspending fluid and allowing them to settle slowly under their own weight prior to establishing temperature control at the precise neutral-buoyancy point. This scheme served to minimize the introduction of air into the suspension. Subsequently, each suspension was aggressively mixed so as to distribute the suspended particles uniformly throughout, after which the suspension was set aside to allow any entrapped air bubbles sufficient time to escape. Following this quiescent period the suspensions were remixed, care being taken to avoid reintroducing any air bubbles.

Experiments were performed in covered cylindrical glass columns, 146 mm in inner diameter and 558 mm in height. Vertical guide tubes were set into the centres of the column lids. Their presence assured release of the falling ball along the axis of the column. Columns were placed in a water-filled tank connected to a water bath and temperature controller, and the suspensions allowed to thermally equilibrate for at least 24 hours prior to performing any experiments. Temperature traverses in the suspensions revealed variations of no more than $\pm$0.03 °C within the viewing area.

The falling balls used in our experiments consisted of 3.18, 6.35, and 12.7 mm brass spheres, as well as 1.59 mm tungsten carbide spheres (Ball and Roller Division of

† Professor M. Gottlieb (Ben Gurion University) was kind enough to test this fluid for viscoelastic properties, thereby establishing its Newtonian nature under the conditions encountered in our experiments.

Hoover, Inc., Hartford, CT) and 12.7 mm aluminium spheres (Small Parts, Miami, FL), whose respective densities were 8.56, 14.9, and 2.71 g cm^{-3}.

2.2. *Experimental procedure*

It is difficult to overemphasize the care necessary to achieve reproducibility when performing dispersion experiments. Previously established experimental protocols (e.g. Milliken *et al.* 1989*a*), while furnishing reproducible settling velocities averaged over a number of experiments, did not, however, yield reproducible variances. This was evidenced by comparing the ratio of variances observed in two apparently equivalent sets of dispersion experiments with a standard F-test value at the 95% confidence limit. That the observed ratio consistently exceeded this 95% confidence value led us to reject the hypothesis that the variances were equal. The source of the problem was eventually traced to the fact that even small variations in temperature, causing only 1–2% differences in the average settling velocity of the ball, could cause differences of as much as 60 to 200% in the horizontal and vertical dispersivities! To better understand the source of these temperature variations and their impact upon the measured dispersivities, the sequence of events composing an experiment will be outlined, followed by a description of the protocol eventually adopted to obtain reproducible variances lying within an acceptable range.

Prior to an experiment, the mass and diameter of the falling balls were determined to within ± 0.2 mg and ± 0.005 mm, respectively. Subsequently, the ball was placed into the water bath so as to allow it to thermally equilibrate with the suspension prior to performing an experiment. Each experiment consisted of six phases: (i) ball release; (ii) waiting for the ball to reach the viewing area; (iii) recording the ball trajectory using the cameras and strobes; (iv) waiting for the ball to reach the bottom of the cylinder after exiting the viewing area; (v) stirring the suspension; (vi) waiting 5–10 mins before repeating the cycle.

Temperature effects were established to be of extreme importance when measuring the second moments of the ball position, especially at the lowest solids concentration, where the magnitudes of the variations were small compared with the average distance settled by the ball. Operating the strobes and stirring the suspension during each experiment added thermal energy to the suspension. Accordingly, the first few experiments performed at the beginning of each day (or after any break of more than 20 min in performing the experiments) saw a rise in the temperature of the suspension, ultimately reaching a higher steady-state temperature than existed initially. This change in temperature was normally 0.1–0.3 °C. These temperature fluctuations, in turn, affected the instantaneous ball-position measurements, creating effects of sufficient magnitude to mask the dispersivities sought.

To reproducibly measure the second moments (say, to within 10–40%), the effects of viscous and thermal heating accompanying each set of experiments were accommodated by physically simulating the experiments until the new higher steady-state temperature appropriate to the actual experiment was reached. For each ball size at each concentration, a few balls would be dropped to estimate how long the experiments would last. Then, at the beginning of each day (or after any break in the experiments lasting 20 min or longer), the suspensions were stirred and the strobes activated for the appropriate amount of time, as if data were actually being taken. This continued until a steady temperature was reached. Basically, this prevented data from being taken during the temperature transients mentioned above, and resulted in reproducible ratios within the standard F-test 95% confidence limits.

To track the settling balls, a high-speed video recorder (NAC's HSV-400^{TM} (Bur-

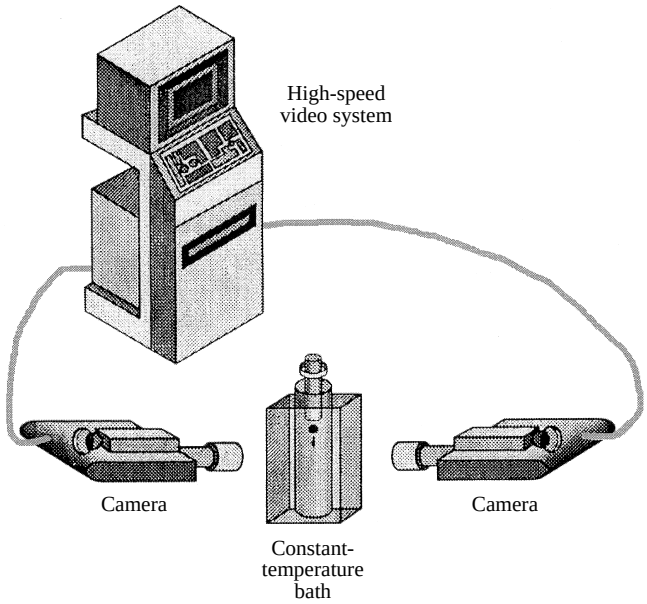

FIGURE 1. An example of the apparatus used to track a ball settling through a transparent suspension.

bank, CA)) was used. This recording scheme served to: (i) minimize systematic errors in spatial and temporal resolution; (ii) allow similar data analysis procedures to be used for both the transparent and opaque suspensions; (iii) store archival data for future review. Displaying two synchronized images from separate cameras on each frame, in combination with uniform spatial and temporal resolution of each image, served to minimize systematic errors. The two cameras were placed roughly 90° apart in a horizontal plane in order to achieve uniform accuracy in the two horizontal directions. A diagram of the experimental apparatus is shown in figure 1. Settling spheres were tracked in camera coordinates using the built-in cursor generators situated on the camera units.

2.3. *Tracking algorithms*

Determining the position of an object in three-dimensional space from two camera images requires that the images fulfil three criteria, namely the existence of: (i) an easily identifiable particle-locator point on each image; (ii) three independent measures of the object's position among the two images; (iii) a mathematical model relating the independent measures to the actual position of the object. The centre of the ball easily satisfies the first criterion, whereas the use of two non-collinear camera views, which furnish four measures of the sphere's position, fulfils the second. The final criterion was satisfied by employing a variation of an existing model (Walton 1981). By using a reference object, this model relates the horizontal and vertical positions of an object observed in two or more camera views (or its camera-fixed coordinates) to the object's physical position in laboratory-fixed coordinates. Because Walton's (1981) original model was developed for measurements taken in air, he was able to assume linear optics. Here, we modified Walton's model so as to account for nonlinear effects arising from the non-refractive-index-matched interfaces existing within our experiment.

Systematic errors arise when studying refractive-index-matched suspensions as a consequence of the non-index-matched interfaces existing between the following sequential elements: (i) the experimental liquid; (ii) the transparent cylindrical container; (iii) the cooling fluid circulating around the cylinder; (iv) the transparent cooling jacket; (v) the ambient air between the system and camera lenses. By using a carefully chosen set of materials and fluids possessing the same refractive index, the possibility exists of eliminating all non-index-matched interfaces, except for the air/cooling jacket interface. Unfortunately, the latter interface, across which the largest change in refractive index occurs, creates the largest nonlinear response. Accordingly, it was deemed necessary to correct for this nonlinear response rather than attempt to eliminate all possible non-index-matched interfaces.

In calibrating the linear model (Walton 1981), deviations between the measured camera coordinates and those calculated from the known physical coordinates (X, Y, Z) of the reference points, in two perpendicular planes, were observed to be approximately quadratic in the physical coordinates. These errors were equivalent to errors of 2 to 6 pixels in determining the object's centre. (The transparent suspension experiments were recorded using the HSV-400 ™ system, which possessed approximately 300 pixels of vertical resolution in the viewable area of interest.) By adding quadratic terms to Walton's (1981) model, the camera coordinates (T^i, U^i) for the ith camera $(i = 1, 2)$ are given as

$$\left.\begin{aligned} T^i &= \frac{B_1^i X + B_2^i Y + B_3^i Z + B_4^i X^2 + B_5^i Y^2 + B_6^i Z^2 + B_7^i}{B_8^i X + B_9^i Y + B_{10}^i Z + B_{11}^i X^2 + B_{12}^i Y^2 + B_{13}^i Z^2 + 1}, \\ U^i &= \frac{B_{14}^i X + B_{15}^i Y + B_{16}^i Z + B_{17}^i X^2 + B_{18}^i Y^2 + B_{19}^i Z^2 + B_{20}^i}{B_8^i X + B_9^i Y + B_{10}^i Z + B_{11}^i X^2 + B_{12}^i Y^2 + B_{13}^i Z^2 + 1}. \end{aligned}\right\} \tag{2.1}$$

To determine the twenty unknown coefficients B_j appearing above, at least ten reference points whose physical coordinates (X, Y, Z) are known are needed for each camera view (for which the T^i and U^i can be measured.) These points must be non-coplanar, though they need not be the same points for both screens because the equations for the camera coordinates are not coupled between cameras. However, in our experiments evenly distributed points in two perpendicular planes were used. These points spanned the common volume imaged by the two cameras.

Once the model was calibrated, determination of the three-dimensional position (X, Y, Z) of an object from its camera coordinates, namely (T^1, U^1) and (T^2, U^2), was achieved by rearranging the four resulting nonlinear equations (one set of the above equations for each camera) into quadratic polynomials in X, Y and Z by multiplying each set of equations by their common denominator. These new nonlinear equations were solved using a standard Newton–Raphson technique to determine the best-fit values of (X, Y, Z).

Twenty points were used to determine the unknown coefficients in equation (2.1), following which an additional sixteen points were used to check the accuracy of the algorithm. For a viewing area with a length of 100 mm, corresponding to 300 pixels in the camera image, the new algorithm gave an accuracy of ± 0.3 mm or about 0.3% of the total field of view. Errors of this magnitude are equivalent to an error of one pixel or less in estimating the screen coordinates. Hence, this model appears to correct for the systematic errors of 2 to 6 pixels encountered when using Walton's linear algorithm.

Our algorithm shares with Walton's the ability to handle an arbitrary number of camera views, provided that every point of interest always lies within view of at least

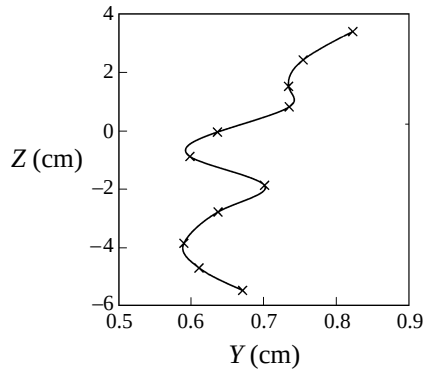

FIGURE 2. A typical trace for a 3.2 mm ball falling through a suspension of neutrally buoyant 3.2 mm spheres, with $\phi = 0.50$. The horizontal axis has been expanded for clarity. A cubic-spline curve (the solid curve) has been fitted to the data.

two of the cameras. Within the resolution of cameras used, this algorithm accurately locates the ball's position without having to place the cameras in precise positions and orientations relative to each other, or to the cylinder containing the suspension. Although the cameras can be located at an arbitrary angle with respect to each other, the best overall accuracy with two cameras is obtained from the conversion routine via use of perpendicular images. With two roughly perpendicular camera views, the two screens had in common one of the three physical directions. This direction (the vertical Z-direction in our experiments) typically gave rise to a slightly smaller uncertainty, since each camera measured the vertical position.

3. Analysis of fully three-dimensional paths

Establishing whether or not a ball settling through a neutrally buoyant suspension behaves in a Fickian manner – and, if so, determining the concomitant vertical and horizontal dispersivities – requires knowledge of the ball's three-dimensional trajectory as a function of time. It is clear from the example shown in figure 2 of a falling ball's trajectory that a ball does not generally settle uniformly through the suspension. Because the ball's path appears stochastic in nature, the moments of the ball's settling path were used to characterize the interactions of the falling ball with the suspension.

The first and second central moments of a ball's trajectory are, respectively, represented by the vector

$$\langle \tilde{\boldsymbol{r}}(\tau) \rangle \stackrel{\text{def}}{=} \frac{1}{N} \sum_{i=1}^{N} [\boldsymbol{r}(t_i + \tau) - \boldsymbol{r}(t_i)] \equiv \bar{\boldsymbol{U}} \tau \tag{3.1}$$

and the dyadic

$$\mathbf{s}^2(\tau) \stackrel{\text{def}}{=} \langle \tilde{\boldsymbol{r}}(\tau) \tilde{\boldsymbol{r}}(\tau) \rangle - \langle \tilde{\boldsymbol{r}}(\tau) \rangle \langle \tilde{\boldsymbol{r}}(\tau) \rangle, \tag{3.2}$$

with

$$\langle \tilde{\boldsymbol{r}}(\tau) \tilde{\boldsymbol{r}}(\tau) \rangle = \frac{1}{N-1} \sum_{i=1}^{N} [\boldsymbol{r}(t_i + \tau) - \boldsymbol{r}(t_i)] [\boldsymbol{r}(t_i + \tau) - \boldsymbol{r}(t_i)], \tag{3.3}$$

in which $\boldsymbol{r} = (X, Y, Z)$ is the instantaneous position vector of the centre of the settling ball, $\tilde{\boldsymbol{r}}(\tau) = \boldsymbol{r}(t_i + \tau) - \boldsymbol{r}(t_i)$ is the vector displacement of $\boldsymbol{r}$ over the sampling time τ,

and $\bar{\boldsymbol{U}}$ is the mean settling velocity vector of the ball. For a purely random or Fickian process, the dyadic $\boldsymbol{s}^2$ is related to the dispersivity dyadic $\boldsymbol{D}$ by the expression

$$\boldsymbol{s}^2(\tau) = 2\boldsymbol{D}\tau + \boldsymbol{E}, \tag{3.4}$$

where $\boldsymbol{E}$ is the variance caused by experimental uncertainties in measuring ball positions and times.

In using equations (3.1) and (3.4) all experiments performed for a given size of settling sphere at a given concentration are assumed to be equivalent. Additionally, taken collectively, the experiments are assumed to represent an adequate sampling of the physical processes governing motion of the settling ball. Finally, the physical process is assumed to be independent of the position $\boldsymbol{r}$ of the ball within the cylinder. This last assumption is equivalent to assuming that wall effects can be ignored and that the suspended particles are randomly and uniformly dispersed.

The validity of the first two assumptions is confirmed by the reproducibility of the variances between two otherwise identical sets of experiments. Mondy, Graham & Jensen (1986) showed that a suspension can be treated as an effective Newtonian fluid continuum insofar as the average falling-ball settling velocity is concerned; moreover, Newtonian wall-effect corrections derived for homogeneous fluids (Happel & Brenner 1983) were also shown by Mondy *et al.* (1986) to be equally appropriate for suspensions. As the instantaneous settling velocity of a ball through a Newtonian fluid contained in a circular cylinder depends upon the radial position of the ball (Hirschfeld, Brenner & Falade 1984), variations in its horizontal position necessarily give rise to concomitant variations in its vertical settling velocity. However, the magnitude of these variations for a ball one-third of the distance from the centreline to the wall was estimated to be less than 1% for the range of falling-ball sizes used in this study. As such, the contribution of these wall effects to the variances may be neglected. For additional details relating to the validity of these assumptions see Abbott (1993).

Because results for the three orthogonal directions should be (and were found to be) independent of each other, only the diagonal terms in the dyadic variance are non-zero. Furthermore, since the dyadic variance is, by symmetry, transversely isotropic with respect to the direction of gravity, it is necessarily of the form

$$\mathbf{s}^2 = \boldsymbol{i}_z\boldsymbol{i}_z s_v^2 + (\boldsymbol{i}_x\boldsymbol{i}_x + \boldsymbol{i}_y\boldsymbol{i}_y)s_h^2, \tag{3.5}$$

where $(\boldsymbol{i}_x, \boldsymbol{i}_y, \boldsymbol{i}_z)$ are unit vectors in the respective (X, Y, Z) directions, and the scalars s_v^2 and s_h^2 represent the respective vertical and horizontal variances.

Although equation (3.4) holds for a Fickian process, any physical process is necessarily deterministic rather than random when viewed on a time scale short enough to reflect the initial conditions. And on this time scale the variance will necessarily display quadratic temporal growth. On an intermediate time scale, however, a transition occurs between this short-time quadratic behaviour and the asymptotic long-time linear behaviour. (See equation (3.10) *et seq.*)

The following subsection describes how the vertical and horizontal variances were determined from the ball trajectories. Subsequently, a scheme is outlined indicating how the corresponding dispersivities were determined from these data.

3.1. *Determining the variances*

Each experiment consisted of tracking a falling ball and recording its position at prescribed time intervals as it traversed a fixed viewing area. Experiments for each specified ball size and suspension concentration were replicated at least 100 times.

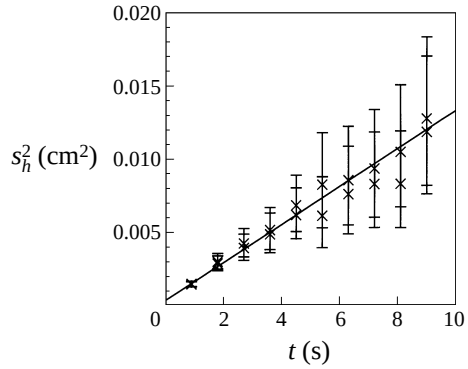

FIGURE 3. Horizontal variance as a function of time for a 6.35 mm settling ball in a 30% suspension of 3.18 mm spheres. The vertical lines represent 95% confidence limits about the two horizontal directions. These data have been fitted by a linear temporal relationship to determine the dispersivity.

When all the data collected in this fashion were used in equation (3.2), in addition to the short-time quadratic behaviour, a long-time decrease in the variances was also observed. This long-time behaviour is caused by using all the data, which prejudiced the sampling of the distribution.

Let t_m denote the minimum time interval required for a ball to settle through the viewing area. Sampling every ball's trajectory only for this amount of time does not, in any way, prejudice the sampling. However, a pseudorandom Gaussian model used to simulate our experiments displayed the observed long-time decrease in the variances after a time t_p, where t_p was chosen such that only 10% of the falling balls took less time than t_p to settle through the viewing area. Hence, this decrease in variance constituted an artifact of the method used to analyse the experiments. In our experiments, for a given falling-ball size and density, trajectory sampling was normally done only until time t_m, but never longer than time t_p.

3.2. *Dispersivity for uncorrelated data*

Examination of the horizontal variances, typified by those shown in figure 3, reveal these to be linear functions of time. This implies that successive displacements as a function of time are uncorrelated, and hence independent of each other. As such, these variances may be regarded as arising from a Fickian process. This graph is the result of 100 ball trajectories, which was the minimum number of balls dropped.

With the positional data uncorrelated as above, the dispersivity D_h is defined as

$$2D_h\tau_i + E_h = s^2_{h,i}(\tau) + \epsilon_i, \tag{3.6}$$

where E_h represents an estimate of the experimental uncertainty, and ϵ_i the uncertainty in the measured variances arising both from experimental uncertainty and the random nature of the process. If these uncertainties are approximately Gaussian, the uncertainty arising from the random nature of the process is then described by the relative bounding values of $\chi^2_{0.025,n_i}$ and $\chi^2_{0.975,n_i}$ as 95% confidence limits, where n_i is the number of displacements used to form the average at τ_i.

Because the uncertainty in the variances is not constant, but varies as indicated in equation (3.6), a weighted least-squares analysis is appropriate using weight factors of $W_i = (\chi^2_{0.975,n_i}/n_i - 1)$. This is equivalent to minimizing the following expression with

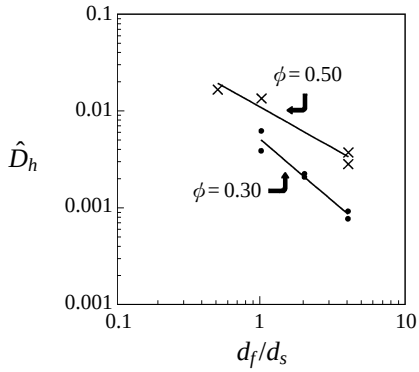

FIGURE 4. Horizontal dispersivity as a function of falling-ball diameter d_f for suspensions of $d_s = 3.2$ mm spheres with $\phi = 0.30$ and 0.50. The most notable trend is that the dimensionless dispersivity $\hat{D}_h$ decreases with increasing d_f/d_s. For $\phi = 0.15$, horizontal variances were not significantly different from the experimental uncertainties; therefore no horizontal dispersivities could be calculated.

respect to D_h and E_h:

$$\sum_{i=1}^{P}(2D_h\tau_i + E_h - s_{h,i}^2)^2 W_i^{-2}. \tag{3.7}$$

3.3. *Horizontal dispersivities*

Use of equation (3.7) and the subsequent equation (4.2) (upon replacing the subscripts v with h in the latter) allows the dimensionless horizontal dispersivities $\hat{D}_h$ to be determined as functions of d_f/d_s and ϕ.

Horizontal variances observed for the various d_f/d_s values investigated at $\phi = 0.15$ did not differ significantly from the experimental error; consequently, no horizontal dispersivities could be calculated at this concentration. However, as shown in figure 4, horizontal dispersivities could be determined for $\phi = 0.30$ and 0.50, at which concentrations the variances significantly exceeded the experimental error. In figure 4, at each ball size ratio there are two data points, these being derived from each of the two perpendicular horizontal directions. (For the two smaller falling-ball sizes at $\phi = 0.50$, the two data points appear as a single point in the figure owing to their closeness.) The ball motions in each of these two directions were found to be uncorrelated, i.e. independent. The resulting dispersivities agree with each other to within experimental uncertainty, which verifies the transversely isotropic assumption made in equation (3.5).

These dispersivities can be seen to decrease with increasing d_f/d_s. A power-law fit of the data yielded the following empirical relations:

$$\hat{D}_h = 0.00502(d_f/d_s)^{-1.27} \quad (\phi = 0.30), \tag{3.8}$$

$$\hat{D}_h = 0.0108(d_f/d_s)^{-0.840} \quad (\phi = 0.50). \tag{3.9}$$

3.4. *Dispersivity for correlated data*

Examination of the vertical variances, similar to those data shown in figure 5, revealed a nonlinear functional dependence upon time for short times, thereby necessitating use of a nonlinear model to determine the vertical dispersivity coefficient from these

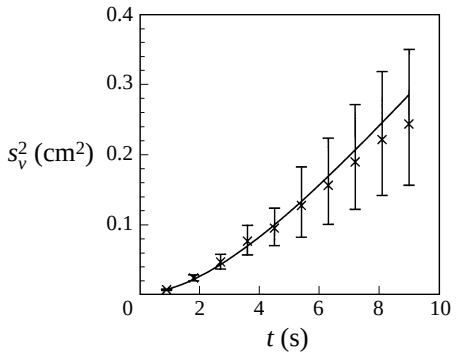

FIGURE 5. Vertical variance vs. time for a 6.35 mm diameter ball falling in a 30% suspension of 3.18 mm diameter spheres. The best fit of equation (3.10) is shown by the solid line.

data. The source of this short-time nonlinear behaviour lies in the deterministic phase preceding that at which the random component of the overall process dominates.

The observed nonlinear behaviour did not arise from inertial forces in our experiments, a fact that was verified by varying the density of the 12.7 mm diameter settling balls in the $\phi = 0.50$ suspension. In particular, by using aluminium and brass spheres, it was established that the variances were statistically independent of falling-ball density (when the times were rescaled with their respective average settling velocities). This suggested that the source of the nonlinearity lay in the change in local geometry of the suspension with time as the ball penetrated the suspension locally, rather than being a rate-related phenomenon. In fact, we believe the relaxational time scale quantifying this nonlinear behaviour to be the characteristic time needed for the settling ball to change its local environment.

Even well-mixed suspensions of spheres display local fluctuations in suspended particle concentration. A falling ball encountering a dense cluster of suspended particles is observed to suffer a marked decrease in its settling velocity. As a consequence, a ball needs to settle through a distance equal to several ball diameters after encountering the cluster before returning to approximately the same velocity it had upon originally approaching the dense cluster. The time scale required for the ball to sample such local concentration fluctuations is of the correct order-of-magnitude to explain the deterministic effects observed in our variance data, as shown by the arguments advanced in the Appendix. The net effect of these arguments is to quantify the functional dependence of the variances upon time by the following relaxation-time model:

$$s_v^2(\tau) = 2D_v\tau - \frac{2D_v}{\alpha}[1 - \mathrm{e}^{-\alpha\tau}] \,, \tag{3.10}$$

with α^{-1} a relaxation time. Arguments outlined in the Appendix suggest that α should scale with $\overline{U}/d_f$. A best fit of the existing data to this model yielded

$$\alpha \approx \frac{0.2\overline{U}}{d_f} \,. \tag{3.11}$$

For short times ($\alpha\tau \ll 1$), equation (3.10) reduces to

$$s_v^2(\tau) = \alpha D_v \tau^2, \tag{3.12}$$

which represents a deterministic process, whereas for times such that $\alpha\tau \gg 1$,

$$s_v^2(\tau) = 2D_v\tau, \tag{3.13}$$

which represents classical Fickian behaviour.

Use of equation (3.11) for α permits D_v to be estimated from any set of vertical variances. Including the experimental error E_v in measuring the vertical positions, together with the varying confidence limits bounding the measured variances, enabled a weighted-least-squares curve to be fitted to the variances s_v^2 as a function of time τ. This is equivalent to minimizing J with respect to D_v and E_v in the following relation:

$$J = \sum_{i=1}^{P} \left\{ 2D_v\tau_i - \frac{2D_v}{\alpha}(1 - \mathrm{e}^{-\alpha\tau_i}) + E_v - s_{v,i}^2 \right\}^2 W_i^{-2}. \tag{3.14}$$

To establish the confidence limits on D_v, a standard nonlinear technique (Draper & Smith 1981) was used to determine the confidence limit on J. This limit (J_F) depends on the minimum value ($J_{\min}$) of J and a function derived from the F-test. The result is

$$J_F = \left(1 + \frac{2}{n-2} F_{0.05,2,n-2}\right) J_{\min}. \tag{3.15}$$

Here, $F_{0.05,2,n-2}$ is the F-test value for the 95% confidence limit in comparing a sample with two degrees of freedom (the model with unknowns D_v and E_v) to a sample with $(n-2)$ degrees of freedom (the variance less the number of parameters fitted). By varying D_v, the maximum and minimum values of D_v are then determined, which give $J = J_F$. While this confidence limit is not exact, the values of D_v, α and E_v that yield the same value of J correspond to a single unknown confidence limit, which is near the 95% confidence limit (Draper & Smith 1981).

As can be seen in figure 5, the nonlinear fit appears to overestimate the variance as time increases. As previously remarked, the confidence limits on the variances are not uniform, whence the deviations are not statistically significant when compared with the errors relative to the confidence limits. Additionally, α has been assumed given by equation (3.11). Were the coefficient α appearing in equation (3.10) empirically determined anew for each experiment by the observed short-time behaviour, and D_v by the long-time behaviour, the fit would be much better, albeit less rational in conception.

3.5. *Vertical dispersivity*

Use of the nonlinear relationship (3.14) together with the estimated values of α given by equation (3.11) enables the vertical dispersivities to be determined. Figure 6 reveals that $\hat{D}_v$ decreases with increasing size ratio d_f/d_s at the smaller concentrations ϕ. The lines shown represent the best-fit power-law relationships between $\hat{D}_v$ and d_f/d_s. Davis & Hill's (1992) theoretical analysis for dilute suspensions suggests a first-order inverse dependence of the form

$$\hat{D}_v = 0.67\phi(d_f/d_s)^{-1}. \tag{3.16}$$

This relation appears to be approximately true for the $\phi = 0.15$ suspension, at least when d_f/d_s is of order one, because the experimentally determined relationship is

$$\hat{D}_v = 0.080(d_f/d_s)^{-0.93} \quad (\phi = 0.15). \tag{3.17}$$

Since the $\phi = 0.15$ suspension is not really dilute, and because of the approximate nature of equation (3.16), exact agreement of our data with the dilute theory results is

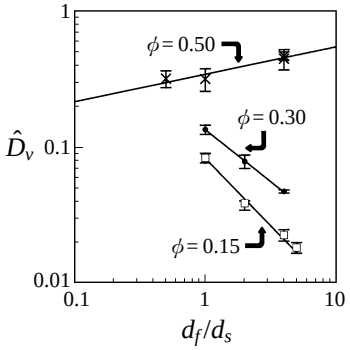

FIGURE 6. Dimensionless vertical dispersivity as a function of relative ball-to-particle size for various particulate concentrations. The most notable trend is that the exponent quantifying the rate at which the dispersivity decreases with relative size goes from near -1 for small ϕ, in accord with theory for dilute systems, to zero or slightly positive for large ϕ. The error bars shown are based on the nonlinear analysis outlined at the end of § 3.4, which assumes α to be given by equation (3.11).

not to be expected. As such, the slight deviation in the exponent from that predicted by Davis & Hill's (1992) calculation is not significant. From a nonlinear error analysis, the value for the exponent lies between -1.46 and -0.67 within 95% confidence limits.

For the suspension composed of 3.18 mm spheres with $\phi = 0.30$, an assumed power-law relationship between $\hat{D}_v$ and d_f/d_s yields, as the best fit,

$$\hat{D}_v = 0.134(d_f/d_s)^{-0.76} \quad (\phi = 0.30). \tag{3.18}$$

Here, the observed exponent differs significantly from the dilute theory predictions of Davis & Hill (1992), as too does the pre-exponential factor, although the latter is of the appropriate order-of-magnitude. Because the confidence limits on the exponent are –1.13 and –0.5, the dilute theory could still be applicable.

At a solids concentration of $\phi = 0.50$, and again for $d_s = 3.188$ mm, $\hat{D}_v$ appears to increase slightly with increasing falling-ball size, although the possibility exists that $\hat{D}_v$ may be a constant. In figure 6, the best-fit line shown passing through the data is given by

$$\hat{D}_v = 0.34(d_f/d_s)^{0.20} \quad (\phi = 0.50). \tag{3.19}$$

The confidence limits on the exponent are respectively –0.08 and 0.5.

The error bars displayed in figure 6 were determined by the method outlined at the end of the previous subsection. As that analysis assumes α to be given by equation (3.11), it does not account for the possible failure of that equation to correctly quantify α. Inclusion of the latter as an empirical parameter to be determined experimentally would reduce the error bars significantly.

Figure 7, which depicts the effect of suspension concentration on vertical dispersivity for the case $d_f = d_s = 3.2$ mm, indicates an approximately linear increase of $\hat{D}_v$ with ϕ, as given by the expression

$$\hat{D}_v = 0.60\phi^{1.08}. \tag{3.20}$$

This linear increase agrees reasonably well with Davis & Hill's (1992) prediction. This agreement is probably fortuitous at the higher concentrations, because the observed size dependence is qualitatively different from that anticipated by their theory.

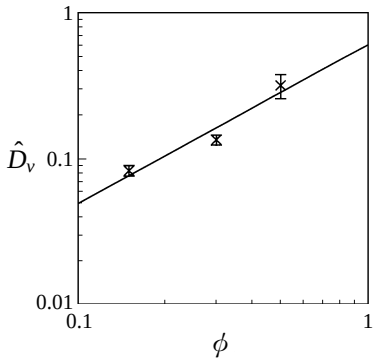

FIGURE 7. Dimensionless vertical dispersivity as a function of volume fraction ϕ of suspended spheres. Because the effect of size is non-uniform, results are shown only for the case where the falling ball possesses the same diameter as the suspended spheres ($d_f = d_s = 3.2$ mm.)

4. Analysis of previous experiments on rod suspensions

Average settling velocities of balls falling through both sphere and rod suspensions, together with their deviations from the mean, have previously been reported over a wide range of parameters (e.g. Fidleris & Whitmore 1961; Mondy *et al.* 1986; Graham *et al.* 1987; Milliken *et al.* 1989*a*, *b*). Because the observed variations in settling velocities are larger than can be explained by experimental errors, these variations may be regarded as systematic, and attributed to the ever-changing interactions occurring among the falling ball and the neutrally buoyant suspended particles. These previous studies represent many years of exacting experimental effort, and our initial objective prior to undertaking the work described in the previous section was to use these studies to estimate the vertical dispersivities. Pioneering sedimentation velocity experiments by Fidleris & Whitmore (1961) on sphere suspensions failed to note any variations in the measured settling velocities arising from the discrete nature of their suspensions. Later work by Mondy, Graham and coworkers (Mondy *et al.* 1986; Graham *et al.* 1987), also on sphere suspensions, did not provide the rigorous temperature control that we now know to be essential for performing reproducible, physically meaningful dispersion experiments. The subsequent studies of Milliken *et al.* (1989*a*, *b*) – the first for spheres and rods, and the second for rods alone – represent over two man years of intensive experimental work, with only very small variations in experimental conditions. The physical properties of the fluids, the suspended particles, and the falling balls used in their experiments are described in detail in the latter two publications.

To estimate the vertical dispersivity D_v from Milliken *et al.* (1989*a*, *b*), variances s_v^2 in the vertical position need to be related to the variances s_u^2 in the settling velocities. Variances in the falling ball's settling velocity measured in those studies arose primarily from variations in the time τ needed for the ball to settle across the viewable area. Using these velocities to calculate the velocity variance over that average settling time enables us to relate s_u^2 to s_v^2 by the expression

$$2D_v\tau = s_v^2 \approx s_u^2\tau^2. \tag{4.1}$$

Contributions from either experimental error or deterministic behaviour are assumed to be small, and hence have been neglected in the above equation. It proves convenient to define a dimensionless dispersivity $\hat{D}_v$ as the ratio of the physical dispersivity D_v to the mean settling velocity $\overline{U}$ multiplied by a characteristic length c of the suspended

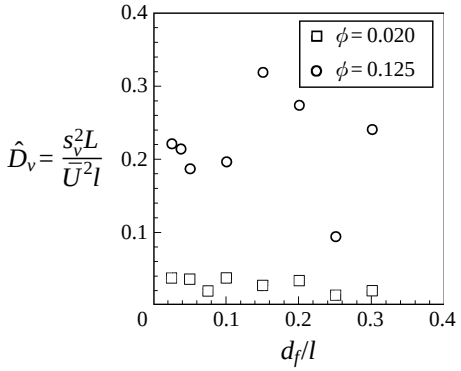

FIGURE 8. Using previously reported (Milliken *et al.* 1989*b*) values of the settling velocities (and their confidence limits) for balls falling in suspensions of rods with $\phi = 0.02$ and 0.125, dimensionless vertical dispersivities $\hat{D}_v$ were calculated as a function of d_f/l. No significant dependence of $\hat{D}_v$ upon d_f/l appears to exist. Note that the dispersivities fail to show a so-called 'small-ball effect', despite the presence of such an effect in the apparent viscosity of the suspension as measured by a falling ball in conjunction with Stokes law (Milliken *et al.* 1989*a*).

particles. For spheres this length is chosen to be the sphere diameter d_s, whereas for rods it is taken to be the rod length l. The variance in the settling velocity is thus related to the dimensionless dispersivity by the expression

$$\hat{D}_v = \frac{D_v}{\overline{U}c} \approx \left(\frac{s_u^2}{\overline{U}^2}\right)\left(\frac{L}{2c}\right), \tag{4.2}$$

where $L = \overline{U}\tau$ is the average distance settled in time τ.

Use of the observed variances in settling velocities reported by Milliken *et al.* (1989*a*, *b*) permits the vertical dispersivities in neutrally buoyant suspensions of both spheres and rods to be estimated via equation (4.2). This technique failed, however, when we attempted to apply it to suspensions of spheres because the reported sphere data, taken from earlier papers, were not uniformly acquired with the same care as were the rod data. Thus, we focused only on the rod data. From figure 8, the non-dimensional vertical diffusivity $\hat{D}_v$ of the ball falling in rod suspensions does not appear to display any statistically significant dependence upon the settling-ball size relative to the rod length, d_f/l, for the two rod concentrations shown. Vertical dispersivities at other concentrations display similar behaviour.

From figure 9 the vertical dispersivity for suspensions of rods appears initially to be proportional to the rod concentration. In preparing this plot we averaged all the dispersion values measured, using different-size settling balls at a given concentration. (From Milliken *et al.* (1989*b*) we know that only the data at the larger volume fractions ϕ deviates significantly from a linear relationship between the relative viscosity μ_r and ϕ. More explicitly, a plot (not shown) of $\hat{D}_v$ vs. the specific viscosity $(\mu_r - 1)$ reveals a linear relationship between $\hat{D}_v$ and $(\mu_r - 1)$ over all concentrations.)

Two fundamental assumptions underlying the above analysis were that: (i) the time τ of the several experiments for a given size of settling sphere was constant; (ii) the dispersion process could be described as purely Fickian. The assumption that τ was constant is included in the approximate nature of equation (4.1), whereas a test of the second hypothesis was confirmed in the preceding section, at least for sphere suspensions.

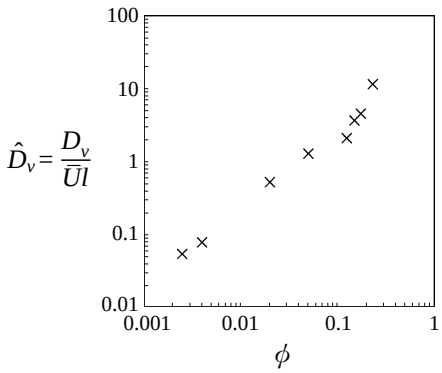

FIGURE 9. Dimensionless vertical dispersivity vs. concentration (ϕ) for rod suspensions. This figure is very close to figure 4 in Milliken *et al.* (1989*a*), which showed the relative viscosity μ_r of the suspension to be linearly dependent upon ϕ over the entire range of values shown, except at the largest value of ϕ.

5. Summary and discussion

In a fundamental sense our falling-ball, quiescent-suspension, dispersion results may be likened to the classical Brownian diffusion results of Perrin (1909, 1910), the latter pertaining to the irregular movement of colloidal particles through macroscopically quiescent fluids. In particular, the stochastic motion manifested by each of these two phenomena arises directly from the fact that the fluid through which the particle moves is not a true continuum, but rather possesses a discrete or granular structure at a 'microscopic' sub-continuum level. Indeed, these two types of experiments differ in principle only in that the force animating the tracer particle is extrinsic in our gravity-driven case whereas it is intrinsic in Perrin's case, arising from the thermal molecular motions of the sub-continuum entities themselves!

In the preceding sections we have demonstrated that the horizontal and vertical fluctuations about the mean position of a ball settling through a quiescent suspension of neutrally buoyant particles is a physically measurable random process, quantifiable by a transversely isotropic Fickian-like dispersivity. Effects of the density and size of the settling ball, as well as the volume concentration, size, and shape of the suspended particles upon the vertical and horizontal components of the dispersivity dyadic have been investigated.

5.1. *Suspensions of spheres*

Within experimental error, the path of a settling ball through a suspension of spheres has been shown to be a Gaussian process for sufficiently long times. This holds even for highly concentrated suspensions, where a fast Fourier transformation analysis (Abbott 1993) reveals no significant periodic motion of the falling ball (whose presence would indicate concentration-induced spatially periodic ordering of the suspended spheres). The magnitude of the vertical dispersivity in concentrated suspensions (with $\phi = 0.30$ and 0.50) has been found to be at least 25 times larger than the corresponding horizontal component, yielding a highly skewed transversely isotropic dispersivity dyadic. However, the fact that the horizontal variances in relatively dilute systems ($\phi = 0.15$) were not significantly larger than the experimental errors furnished a lower limit on the ratio of vertical to horizontal variances of about 10.

Vertical and horizontal dispersivities have also been estimated by Nicolai *et al.* (1996). However, in their experiments the suspended particles were (deliberately) not

neutrally buoyant and hence underwent sedimentation. They reported their results as a function of the ratio of the settling velocity of the tracer particle to the settling velocity of a sedimenting particle. As this ratio increased, their results, however, failed to be correlated by this single parameter. For a ratio of 7, the largest value reported, they estimated the vertical dispersivity to be at least 50 fold greater than the horizontal dispersivity at $\phi = 0.20$. This was the only concentration examined in their study; nevertheless, to the degree that a neutrally buoyant suspension can be compared with a sedimenting suspension, their result agrees qualitatively with ours.

For short times the vertical variances in our experiments did not always initially grow linearly with time, but rather displayed initial quadratic growth behaviour, indicating that motion of the falling ball is deterministic for these short times. To test whether inertial effects caused this anomalous non-stochastic behaviour, the density of the falling ball was varied. Inertial effects were thereby excluded as the source of the implied deterministic behaviour. Rather, the correlated behaviour implicit in the nonlinear temporal variance data is believed to be related to the time interval it takes for the falling ball to change its local particulate environment.

In order to separate the random and deterministic contributions to the observed vertical variances, we hypothesized the existence of a relaxation time α^{-1}, related to the time scale on which the settling ball undergoes a sensible change in its particulate environment. Because the settling ball tends to drag the suspended particles along with it, this time scale was experimentally observed to be about 5 ball diameters divided by the mean velocity of the ball. However, since this relaxation time does not account for the relative size of the suspended spheres, it should be regarded only as a first-order estimate, likely to be valid only when the falling ball and suspended particles are of comparable size.

In suspensions of spheres the vertical component of the falling ball's dimensionless dispersivity $\hat{D}_v$ was observed to decrease with increasing ball size at the lower concentrations studied. In moderately concentrated suspensions ($\phi = 0.15$), the scaling of this dispersivity with the relative size d_f/d_s of the falling ball to the suspended spheres agreed well with the dilute suspension theory of Davis & Hill (1992) for the case where $d_f/d_s = O(1)$. As particle concentration increased, however, the functional dependence of $\hat{D}_v$ upon d_f/d_s diminished, ultimately becoming either independent of the size ratio at $\phi = 0.50$ or increasing slightly. The transition between the dilute and concentrated behaviour appears smooth, suggesting that as the concentration of suspended particles increases the ball's hydrodynamic interactions with the suspension becomes increasingly dominated by particle/particle interactions in contrast with ball/particle interactions. Finally, the dimensionless vertical dispersivity increases approximately linearly with ϕ at constant d_f/d_s.

Davis & Hill's (1992) calculations for suspensions of spherical particles include only two-body effects, and hence predict no horizontal dispersivity as a consequence of the reversible nature of these two-body hydrodynamic interactions. As horizontal variance estimates require accounting for three-body interactions (or irreversible two-body interactions), horizontal dispersivities were not expected to be as large as their vertical counterparts, nor to display the same functional dependence upon d_f/d_s or ϕ. Our experimental observations are consistent with these facts. Explicitly, the non-dimensional horizontal dispersivity $\hat{D}_h$ decreased with increasing ball size, although at a rate that diminished with increasing particle concentration. However, the relative effect was always greater than for the comparable vertical dispersivity $\hat{D}_v$. A trend analysis (Abbott 1993) comparing the two dispersivities suggests that the magnitude

of the horizontal dispersivity might actually exceed that of the vertical dispersivity for sufficiently small size ratios d_f/d_s. We suspect, however, that a different mechanism exists for falling balls much smaller in diameter than the suspended spheres (Milliken *et al.* 1989*a*), a phenomenon which would invalidate extrapolating our results into that region.

5.2. *Suspensions of rods*

In suspensions of rods, $\hat{D}_v$ appears to be independent of the size of the settling sphere. For $\phi = 0.15$, $\hat{D}_v$ is about four times larger than the comparable value for spheres. This comparison of dimensionless dispersivities is, however, based upon different length scales, namely the respective rod length and suspended sphere diameter in the two cases. Hence, while the factor of four is not overly significant (considering the assumptions made in analysing the rod data), the fact that the length of the rods replaces the diameter of the spheres as the characteristic length scale makes the actual variances in rod suspensions (over the time interval required for a ball to settle a fixed distance) about 40 times greater than for comparable sphere suspensions.

Considering the large role that the postulated deterministic behaviour plays in estimating dispersivities from the variance data, one might question the reliability of dispersivity estimates derived in this fashion. (For suspensions of spheres such estimates did not display any consistent trends with respect to falling-ball size or suspension concentration.) Two major reasons for having confidence in the rod results are that: (i) the rod dispersivities were forty times greater than for spheres; (ii) the diameter of the falling ball was always less than the length of the suspended rods. The first reason allows small perturbations in experimental conditions (changes in temperature, stirring methods, etc.) to be neglected, as they do not contribute significantly to the measured dispersivities, while the second reason allows deterministic effects to be neglected. To resolve this issue unequivocally, complete falling-ball trajectories would have to be determined for suspensions of rods.

In rod suspensions, $\hat{D}_v$ increases linearly with the specific viscosity of the suspension. Because the suspension viscosity for all but the highest concentration is also approximately linear in ϕ, this trend parallels the theoretically predicted behaviour (Davis & Hill 1992) for dilute suspensions of spheres.

This work was sponsored by the US Department of Energy at Los Alamos National Laboratory under contract W-7405-ENG-36 with the University of California, at Sandia National Laboratories under contracts DE-AC04-76DP00789 and DE-AC04-94AL85000, and at MIT under contract DE-FG02-88ER13896. The authors gratefully acknowledge partial support for this work by the US Department of Energy, Division of Engineering and Geosciences, Office of Basic Energy Sciences.

Appendix. Derivation of equation (3.11)

Arguments are advanced in what follows in support of equation (3.11) as arising from local inhomogeneities in the spatial distribution of suspended particles. To model this behaviour consider the following force balance on the settling ball:

$$F_B = F_D + F_A \,. \tag{A 1}$$

Here, with an obvious choice of notation, F_B, F_D, and F_A are respectively the body, drag, and inertial acceleration forces; explicitly,

$$F_B = mg, \tag{A 2}$$

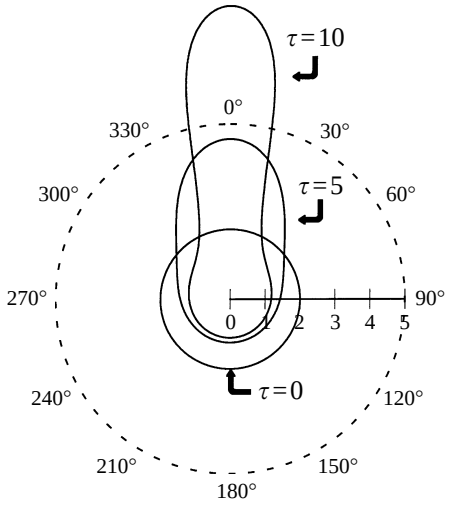

FIGURE 10. The axisymmetric deformation relative to the ball's motion of an initially spherical shell of fluid around a falling ball (not shown) of unit radius. The fluid shell is initially concentric with the ball, but twice the ball's diameter. Different curves represent the deformation of the shell at various times $\tau = \frac{1}{2}nd_f/\overline{U}$ needed for the ball to move the number n of sphere diameters noted on the figure.

$$F_D = 6\pi\mu a U, \tag{A 3}$$

$$F_A = m\frac{\mathrm{d}U}{\mathrm{d}t}\ . \tag{A 4}$$

Our experiments correspond to the regime for which the inequality $F_A \ll F_D$ holds. Elimination of F_A from equation (A 1) yields

$$\frac{U(t)}{\overline{U}} = \frac{\overline{\mu}}{\mu(t)}\ . \tag{A 5}$$

Here, $U(t)$ represents the instantaneous velocity of the falling ball, whereas $\mu(t)$ and $\overline{\mu}$ are the local and average effective viscosities of the suspension, respectively.

As the falling ball encounters local fluctuations in suspended-sphere concentration its resistance to motion necessarily varies too with the local instantaneous configuration of suspended particles. Earlier workers demonstrated that, on average, suspensions behave rheologically as hypothetical one-phase Newtonian fluids with effective fluid properties (e.g. Fidleris & Whitmore 1960; Mondy *et al.* 1986). Therefore, we assume that Stokes flow around the falling ball, as shown in figure 10, is a valid model of the actual flow field in a time-averaged sense.

Consider the evolution in time of a spherical shell of fluid surrounding a ball settling in a Newtonian fluid. As shown in figure 10, the initially spherical shell deforms and elongates due to the no-slip condition imposed on the surface of the ball. Observe that after the ball has moved 5 and 10 ball radii a significant fraction of the fluid initially in the shell remains in the neighbourhood of the ball.

A series of calculations was performed to determine the rate at which a falling ball 'forgets' its local environment. Spherical shells of fluid whose centres were initially coincident with the falling ball's centre were subjected to Stokes flow (see figure 10). Of course, not each location has the same relative effect upon the ball's motion. Therefore, each location was weighted with the net effect on the ball's motion of a suspended sphere at that location. Brenner *et al.* (1990), using the method of

reflections, determined this weighting to be $1/r^4$, where r is the radial distance measured from the centre of the falling ball. The results of these calculations reveal that to a high degree of accuracy a falling ball forgets its local environment in an exponential manner; that is,

$$\frac{\mu(t)}{\bar{\mu}} = 1 - \delta e^{-\alpha t} , \tag{A 6}$$

where α^{-1} is an undetermined time constant and δ represents the magnitude of the viscosity fluctuation relative to the average viscosity; explicitly,

$$\delta = \frac{\bar{\mu} - \mu(0)}{\bar{\mu}} . \tag{A 7}$$

This functional form (A 6) is invariant over a reasonable range of shell radii. Substituting equation (A 6) into (A 5) and assuming δ to be small compared with unity yields

$$\frac{U(t)}{\bar{U}} = 1 + \delta e^{-\alpha t} . \tag{A 8}$$

Upon defining the fractional velocity deviation

$$\tilde{U} = \frac{U(t) - \bar{U}}{\delta \bar{U}} , \tag{A 9}$$

it follows that

$$\tilde{U} = e^{-\alpha t} . \tag{A 10}$$

Note that rather general arguments in favour of (3.11) could have been given in terms of the rate at which velocity fluctuations become uncorrelated (see, for example, equation (175) of Chandrasekhar 1943), rather than relying upon the model detailed in this Appendix.

REFERENCES

Abbott, J. R. 1993 Dispersive processes in concentrated suspensions. PhD thesis, Massachusetts Institute of Technology.

Abbott, J. R., Tetlow, N., Graham, A. L., Altobelli, S. A., Fukushima, E., Mondy, L. A. & Stephens, T. S. 1991 Experimental observations of particle migration in concentrated suspensions: Couette flow. *J. Rheology* **35**, 773–795.

Brenner, H., Graham, A. L., Abbott, J. R. & Mondy, L. A. 1990 Theoretical basis for falling-ball rheometry in suspensions of neutrally buoyant spheres. *Intl J. Multiphase Flow* **16**, 579–596.

Chandrasekhar, S. 1943 Stochastic problems in physics and astronomy. *Rev. Mod. Phys.* **15**, 1–89.

Davis, R. H. 1996 Hydrodynamic diffusion of suspended particles. A symposium. *J. Fluid Mech.* **310**, 325–336.

Davis, R. H. & Hill, N. A. 1992 Hydrodynamic diffusion of a sphere sedimenting through a dilute suspension of neutrally-buoyant spheres. *J. Fluid Mech.* **236**, 513–533.

Draper, N. R. & Smith, H. 1981 *Applied Regression Analysis*, Chap. 10. Wiley.

Eckstein, E. C., Bailey, D. G. & Shapiro, A. H. 1977 Self-diffusion of particles in shear flow of a suspension. *J. Fluid Mech.* **79**, 191–208.

Fidleris, V. & Whitmore, R. L. 1961 The physical interactions of spherical particles in suspensions. *Rheol. Acta* **1**, 573–580.

Gadala-Maria, F. & Acrivos, A. 1980 Shear-induced structure in a concentrated suspension of solid spheres. *J. Rheology* **24**, 799–811.

Graham, A. L., Altobelli, S. A., Fukushima, E., Mondy, L. A. & Stephens, T. S. 1991 NMR imaging of shear-induced diffusion and structure in concentrated suspensions undergoing Couette flow. *J. Rheology* **35**, 191–201.

Graham, A. L., Mondy, L. A., Gottlieb, M. & Powell, R. L. 1987 Rheological behavior of suspensions of randomly oriented rods. *Appl. Phys. Letts.* **50**, 127–129.

Ham, J. M. & Homsy, G. M. 1988 Hindered settling and hydrodynamic dispersion in quiescent sedimenting suspensions. *Intl J. Multiphase Flow* **14**, 533–546.

Happel, J. & Brenner, H. 1983 *Low Reynolds Number Hydrodynamics.* Kluwer.

Hirschfeld, B. R., Brenner, H. & Falade, A. 1984 First- and second-order wall effects upon the slow viscous asymetric motion of an arbitrarily-shaped, -positioned and -oriented particle within a circular cylinder. *PhysicoChem. Hydrodyn.* **3**, 99–133.

Leighton, D. T. & Acrivos, A. 1987*a* Measurements of shear-induced self-diffusion in concentrated suspensions of spheres. *J. Fluid Mech.* **177**, 109–131.

Leighton, D. T. & Acrivos, A. 1987*b* The shear-induced migration of particles in concentrated suspensions. *J. Fluid Mech.* **181**, 415–439.

Milliken, W., Gottlieb, M., Graham, A. L., Mondy, L. A. & Powell, R. L. 1989*a* The viscosity–volume fraction relationship of a randomly oriented suspension of rods. *J. Fluid Mech.* **202**, 217–232.

Milliken, W., Mondy, L. A., Gottlieb, M., Graham, A. L. & Powell, R. L. 1989*b* The effect of the diameter of falling balls on the apparent viscosity of suspensions of spheres and rods. *PhysicoChem. Hydrodyn.* **11**, 341–355.

Mondy, L. A., Graham, A. L. & Jensen, J. L. 1986 Continuum approximations and particle interactions in concentrated suspensions. *J. Rheology* **30**, 1031–1051.

Nadim, A. 1988 The measurement of shear-induced diffusion in concentrated suspensions with a Couette device. *Phys. Fluids* **31**, 2781–2785.

Nicolai, H., Herzhaft, B., Hinch, E. J., Oger, L. & Guazzelli, E. 1995 Particle velocity fluctuations and hydrodynamic self-diffusion of sedimenting non-Brownian spheres. *Phys. Fluids* **7**, 12–23.

Nicolai, H., Peysson, Y. & Guazzelli, E. 1996 Velocity fluctuations of a heavy sphere falling through a sedimenting suspension. *Phys. Fluids* **8**, 855–862.

Perrin, J. 1909 Mouvement brownien et realite. *Ann. Chem. Phys.* **18**, 1–114.

Perrin, J. 1910 *Brownian Movement and Molecular Reality*. Taylor & Francis.

Phillips, R. J., Armstrong, R. C., Brown, R. A., Graham, A. L. & Abbott, J. R. 1992 A constitutive equation for concentrated suspensions that accounts for shear-induced particle migration. *Phys. Fluids* A **4**, 30–40.

Walton, J. S. 1981 Close-range cine-photogrammetry: A generalized technique for quantifying gross human motion. PhD thesis, Pennsylvania State University.

Wang, Y., Mauri, R. & Acrivos, A. 1993 The transverse shear-induced liquid and particle tracer diffusivities of a dilute suspension of spheres undergoing a simple shear-flow *J. Fluid Mech.* **327**, 255–272.